Journal of Power Sources 193 (2009) 39–48

Contents lists available at ScienceDirect

Journal of Power Sources

journal homepage: www.elsevier.com/locate/jpowsour

Mixed-reactant, micro-tubular solid oxide fuel cells: An experimental study

N. Akhtar[a,b,*], S.P. Decent[a], D. Loghin[a], K. Kendall[b]

[a] School of Applied Mathematics, University of Birmingham B15 2TT, Birmingham, UK
[b] Department of Chemical Engineering, University of Birmingham B15 2TT, Birmingham, UK

ARTICLE INFO

Article history:
Received 2 October 2008
Received in revised form 3 January 2009
Accepted 8 January 2009
Available online 22 January 2009

Keywords:
Solid oxide fuel cell
Mixed-reactant
Air–fuel mixture
Single-chamber
Micro-tubular

ABSTRACT

Anode-supported, micro-tubular solid oxide fuel cells were prepared and operated, utilizing mixed-reactant (methane and air mixture) supply. The cells were composed of conventional materials, i.e. nickel, yttria-stabilized zirconia (Ni-YSZ) as anode supported material, yttria-stabilized zirconia (YSZ) as electrolyte, and lanthanum strontium manganite (LSM) as cathode material. The cells were operated at various temperatures in between 550 and 800 °C with varying methane/air ratio (1:1–1:4.76). Cell performance was found to be strongly dependent on flow rate and mixing ratio. At 750 °C, the maximum open circuit voltage (OCV) of the cell was 1.05 V at a methane/air ratio of 1:4.76, with a maximum power output of 122 mW cm^{-2}. The degradation test shows 0.05% performance loss per 24 h, thereafter, fluctuations in current density were observed due to oxidation–reduction cycles over nickel surface. It is therefore concluded that although the methane/air ratio of 1:4.76 gives the best performance but the long-term performance is not guaranteed under such conditions.

1. Introduction

Solid oxide fuel cells seem to be attractive due to their numerous advantages e.g. choice in fuel flexibility (hydrogen, natural gas, biogas, diesel, liquefied petroleum gas (LPG), methanol, dimethyl ether (DME) and ethanol), wide range of operation (400–600 °C, using GDC based electrolytes, 600–1000 °C, with yttria-stabilized zirconia (YSZ) based electrolytes), cost effective materials (when operated at intermediate temperatures, 600–800 °C) [1]. Micro-tubular design gives further additional benefits of improved shock resistance, rapid start-up/shut down, high surface to volume ratio and improved thermal cycling performance [2]. Not only this, we have also demonstrated (for the first time) that the micro-tubular cells can be operated on mixed-reactants (air/fuel mixtures). This new research open pathways to solve many of the major problems, for which the solid oxide fuel cell (SOFC) community is currently struggling, such as thermal stresses, carbon deposition on anode, robust sealing materials that can withstand in oxidizing/reducing environment and ensure leak proof cells [3–5].

The concept of operating SOFCs with mixed-reactants is not a new research, there are numerous research papers written so far [6–70]. Most of the researches considered conventional (sandwiched type) design, a few of them focused on co-planar configuration (or surface migration cell) [7,16,17,18,20,22,25,29,30,32,35,49,63,64,66]. Each of these two configurations has its merits and disadvantages, e.g., conventional design is limited by the use of maximum electrolyte thickness, but on the other hand offers two geometrical set-up i.e., perpendicular giving better reactant utilization or parallel offering better hydrodynamics [62]. Co-planar design can offer electrolyte supported cells but the open circuit voltage (OCV) is lower than the sandwiched type design because of parasitic losses associated with intermixing of reactants/products. The short distance between the electrodes necessary for minimizing the ionic current transfer path is the main culprit for such intermixing in the vicinity of electrodes [49]. Also, in both, the sandwiched and the co-planar design, electrodes are open in the air/fuel mixture environment, intermixing via flushing and convection cannot be completely avoided. However, tubular design can offer some advantages:

- Since one of the electrodes is enclosed in the electrolyte thus the parasitic losses can be reduced to a great extent because of negligible convection of the electrochemically-produced hydrogen, carbon monoxide from anode to the cathode.
- The electrode, which is located in the inner side of the tube, will accelerate the flow due to small inner diameter of the tube enclosure, as compared to the outer electrode, which is enclosed in a larger tube (i.e. the gas-chamber tube). Thus, improved mass transfer is expected via forced convection in the inner electrode.
- If the anode is the inner one, the local depletion of fuel will be more by electrochemically-produced water, because the small volume of inner space cannot efficiently replenish the local

* Corresponding author at: School of Applied Mathematics, University of Birmingham, B15 2TT, UK. Tel.: +44 7726 126748; fax: +44 121 4143389.
E-mail address: nxa675@bham.ac.uk (N. Akhtar).

0378-7753/$ – see front matter © 2009 Elsevier B.V. All rights reserved.
doi:10.1016/j.jpowsour.2009.01.032

stream. Cathode as the inner electrode may offer advantage in this case.
- Air/fuel mixture directly supplied to the inner cathode first and then passed to the outer anode (Hibino A-type [41]) can offer better performance.
- Short cells can offer uniform reactant utilization over the cell length.
- Reducing the diameter of the gas-chamber tube downstream will accelerate the flow for the outer electrode, thus improving the mass transport via forced convection.
- The partial oxidation reaction (on which the single-chamber SOFC operates) is an exothermic reaction; cells with anode inside will have higher local temperatures than the outer cathode. This will further dilute the reactants/products at the anode via thermal convection. In this case, anode as outer layer will have lower local temperature due to heat transfer to the surrounding gas mixture and walls of the gas-chamber.
- In case of stack (where the bunch of cells are located in radial direction across a centered cell) with cathode as an outer layer may cause oxygen depletion. In this case the mixture can become rich in fuel, thereby reducing the stack performance. Mixture of anode/cathode outside cells may level this effect.

In order to take benefit from the above discussion, micro-tubular geometry was opted in this study. A three years research project "Mixed-Reactant Solid Oxide Fuel Cells" is now half on its way, aiming at, modeling and experimental activities on single-chamber solid oxide fuel cells [61,62]. In this paper, the concept of mixed-reactant, micro-tubular solid oxide fuel cells has been presented. This paper discusses the experimental work carried out by keeping the following objectives in mind.

2. Objectives

- Simple experimental set-up (using single-chamber), thus eliminating the need for separate channel for air and fuel.
- Focusing on micro-tubular design, which has several advantages over other available designs (e.g. planar, monolithic etc.) such as rapid start-up, mechanically shock resistant etc.
- Focusing on intermediate temperature (550–800 °C) for operation.
- Comparing the reduction methods using hydrogen, methane and methane/air mixtures.
- Comparing the performance using hydrogen, methane and methane/air mixture as fuels.
- Investigating the stability of the cell performance on laboratory scale.

3. Experimental

Nickel oxide, yttria-stabilized zirconia (NiO-YSZ) anode supported micro-tubes with yttria-stabilized zirconia (YSZ) as an electrolyte already coated on top of the existing anode, were supplied by Adaptive Materials Inc. (AMI), USA. These tubes were received as anode supported electrolyte micro-tubes. Two cathode layers were prepared by using the recipe given in [71]. Cathode layer-1 was painted onto the electrolyte later to a length of 30 mm and left to dry overnight. Cathode layer-2 (of same length as of layer-1) was then applied and sintered by using the scheme as shown in Fig. 1. After sintering, approximately 10 mm length of thin electrolyte was carefully removed for current collection from the exposed anode. Afterwards, silver ink was applied to the exposed anode and also in three small segments (3 mm each) at the cathode. The purpose of applying the silver ink was to enhance electrical conductivity of anode/cathode and catalytic activity of the cathode. Finally, one silver wire was wound around the exposed anode to collect current from the anode side and the other was wound around the cathode to complete the electrical circuit. In order to fix the silver-wire on anode, high temperature cement was used as a sealant, which ensures that anode and cathode silver wires are not short-circuited. This completes the cell preparation and corresponding stages are shown in Fig. 2. Table 1 summarizes the dimensions of each layer of the cell and the gas-chamber tube. Fig. 3 shows the cross-section view of the anode-electrolyte-cathode layer.

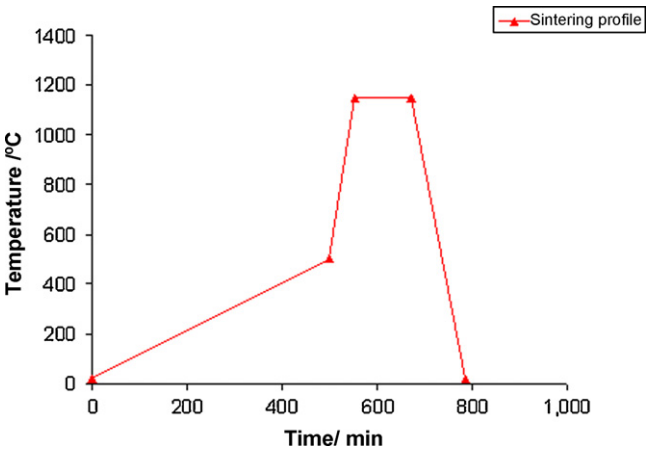

Fig. 1. Sintering profile for cathode.

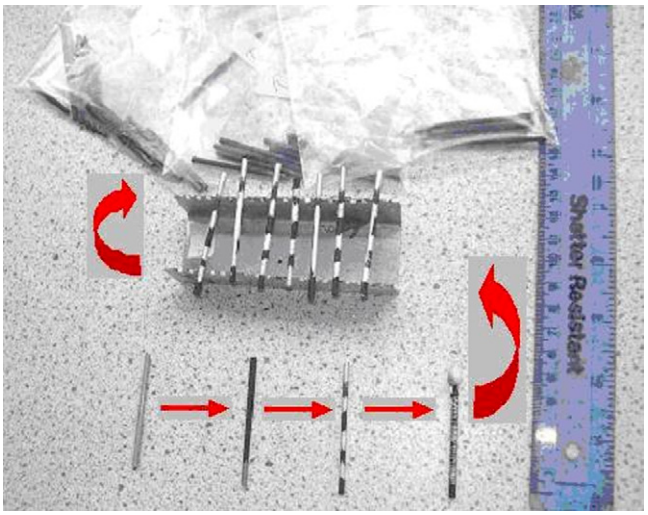

Fig. 2. Stages in cell fabrication.

Table 1
Geometry dimensions.

Dimensions	Value	Units
Gas-chamber length	285	mm
Gas-chamber outer diameter	13	mm
Gas-chamber inner diameter	11	mm
Cell outer diameter	2.0	mm
Cell length	55	mm
Anode thickness	200	μm
Cathode-1 thickness	10	μm
Cathode-2 thickness	40	μm
Electrolyte thickness	15	μm
Cathode active length	30	mm
Active area	1.885	cm^2

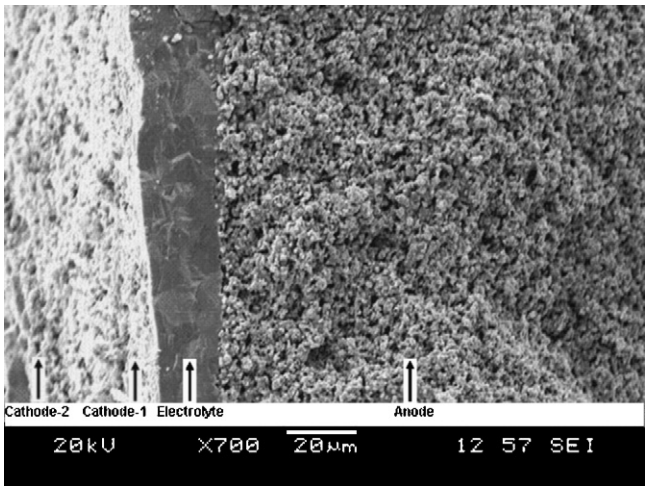

Fig. 3. SEM photograph of anode-electrolyte-cathode cross-section.

The cell was kept in the center of the gas-chamber tube with a holder (Fig. 4). A brick furnace was controlled by a Eurotherm™ 2402 controller with a K-type thermocouple to measure the furnace temperature. Two unit instruments 7300 mass flow controllers were used to control the flow of gases (fuel and air) to the system. The voltage and current data was displayed on a potentiostat which was further manipulated by Microsoft Office Excel programme. The gases used were hydrogen (purity 99.95%), methane (CP-grade) and air (21% oxygen, 79% nitrogen) supplied by British Oxygen Company (BOC).

4. Results and discussion

4.1. Reduction methods

We employed three different reduction mechanisms i.e. hydrogen (20 ml min^{-1}, 800 °C [72]), methane (10 ml min^{-1}, 650 °C [73]) and methane/air mixture (25/60 ml min^{-1}, 750 °C) and the cell's OCV was recorded in-situ. Fig. 5 compares these different reduction schemes and it can be seen that the cell reduction with hydrogen took 50 min and the highest OCV of 1.025 V (with 1050 mA/0.5 V) was recorded in this case. Reduction with methane was not successful, even after 5 h of operation the OCV was only 102 mV. The cell was then taken out of the gas-chamber and it was found cracked. As reported by Shao and co-workers [65] the cell did reduce but was

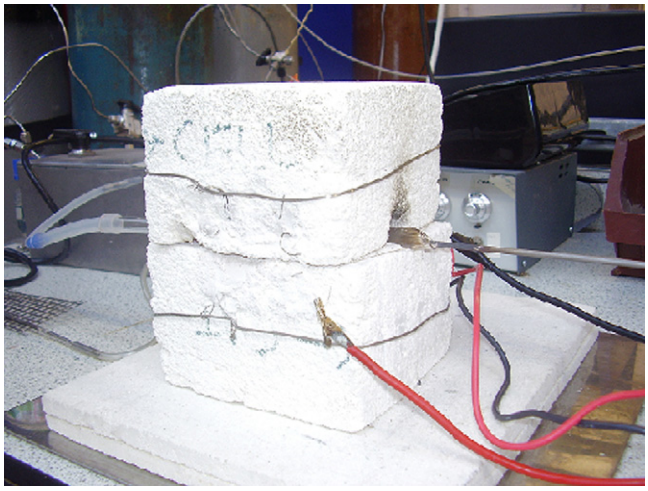

Fig. 4. Experimental set-up.

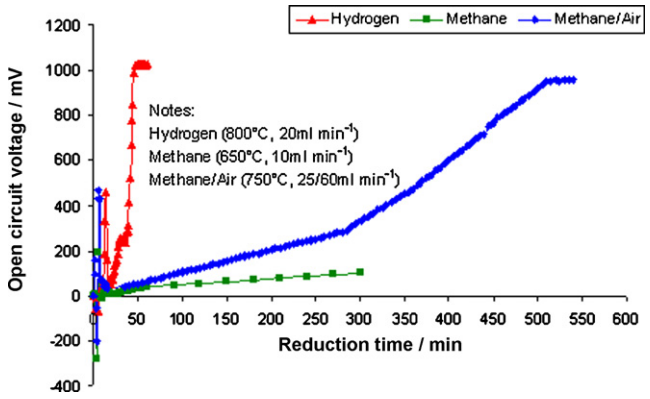

Fig. 5. Comparison of reduction schemes for hydrogen, methane and methane/air mixture as a reducing fuel for anode.

badly damaged by carbon formation over a long period of reduction. We assume the same reason for low OCV and nearly zero current in this condition.

The reduction with methane/air mixture did also work but it was extremely slow, probably due to strong competition between oxygen and fuel reaching the NiO catalyst. It took approximately 9 h to reduce the cell using air/fuel mixture and the OCV recorded thereafter was 960 mV (with 80 mA/0.5 V). We would like to mention here that Shao and co-workers [65] reported a failed reduction using methane/oxygen ratio ($R_{mix} = 1.0$), which is probably due to relatively high amount of oxygen present in their mixture, in contrast to our methane/oxygen mixture ($R_{mix} = 2.0$), which was chosen from a stability study of SC-SOFC [66].

4.2. Effect of mixing ratio

In order to study the effect of mixing ratio on the cell performance, five different methane/air ratios were opted, i.e. 1:4.76, 1:4, 1:3, 1:2 and 1:1. This range was carefully selected by keeping in mind, the window of possible operation (using methane/air mixtures) under single-chamber SOFC conditions. For example, decreasing the ratio below to that of 1:4.76 can cause oxidation of nickel anode (depending upon area ratio of the electrodes) and also the mixture may become explosive (5–15% by volume methane in air is explosive at standard conditions). On the other hand, operations at high methane/air ratios beyond 1:1 can cause severe coking (depending upon area ratio of the electrodes) on nickel anodes [56].

The effect of mixing ratio on the cell performance was observed at different operating temperatures from 550–750 °C. Fig. 6(a–e) shows their effect on *I–V* characteristic of the cell. In all these figures a common trend has been observed showing methane/air = 1:4.76 as the best and 1:1 giving the worst performance. An interesting behavior noted is the marginal increase in performance at methane/air ratio of 1:4.76 with increasing temperature as compared to all other mixing ratios. Though this trend shows that higher air/fuel ratios are better, but nothing can be drawn about stability of the performance from these curves. A detailed stability analysis is therefore necessary to declare them as the best mixing ratios. We would like to mention here that there are several reports [10,11,13,19,22,29,33,38,47,63] stating the best performance was achieved at methane/air ratio of 1:4.76 ($R_{mix} = 1.0$) and also some reports [7,15,17,23,25,26,31,37,63,64,66] focusing at methane/air ratio of 1:2.4 ($R_{mix} = 2.0$). This contradiction depends on many parameters such as electrode microstructure and material, geometrical configuration, reduction technique and the operational temperature. The best performance achieved in our case at methane/air ratio of 1:4.76 could possibly be due to improved oxy-

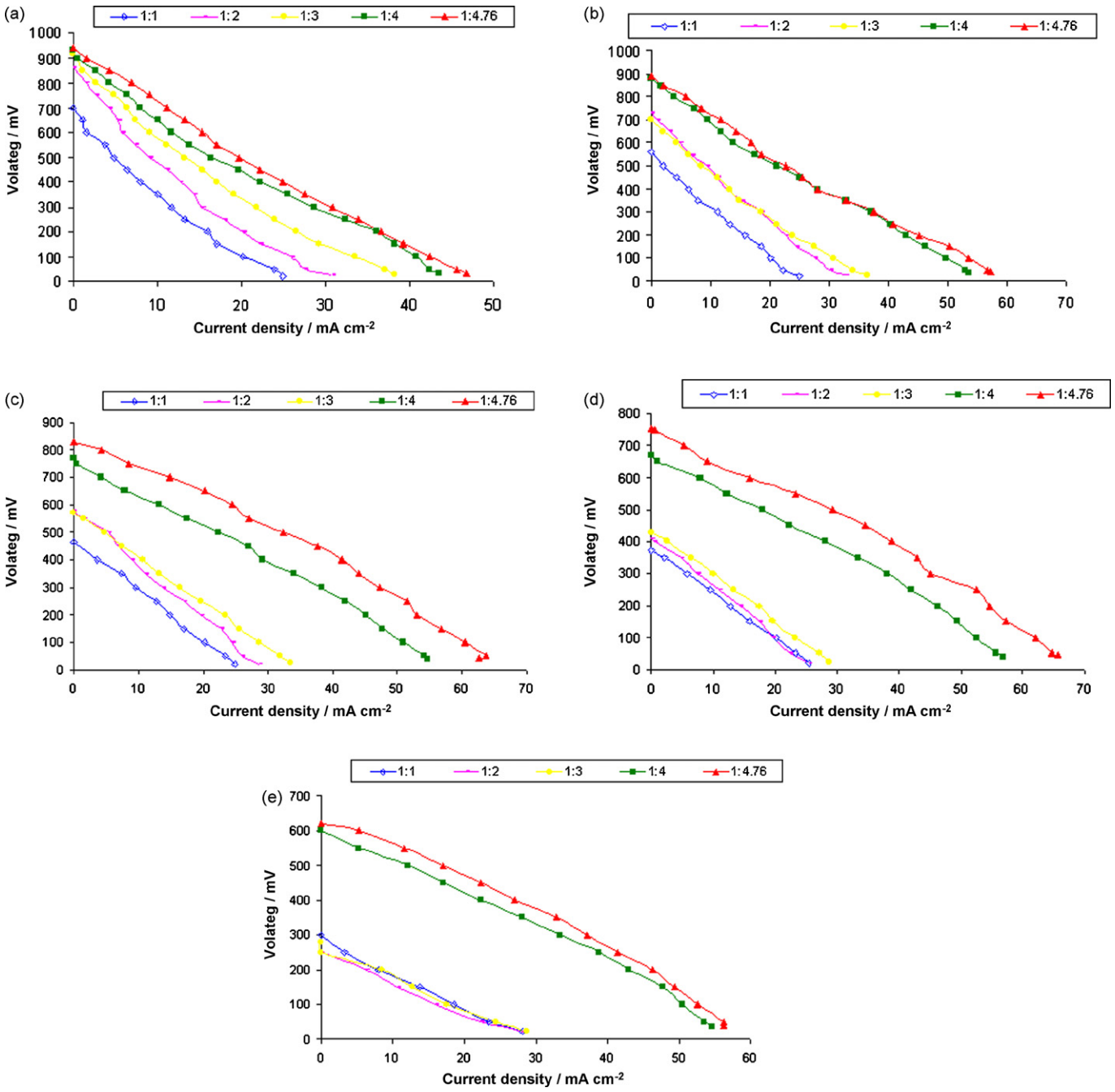

Fig. 6. *I–V* curves at (a) 550, (b) 600, (c) 650, (d) 700, and (e) 750 °C temperatures for various methane/air mixtures (total flow rate = 12 ml min^{-1}).

gen reduction rate at the LSM cathode because of abundant supply of oxygen at these mixing ratios [10].

4.3. Effect of operating temperature

Fig. 7 shows the effect of operating temperature on OCV and the current density at 0.5 V with cell operating at 10/47.6 ml min^{-1} methane/air flow rate. The maximum current density (at 0.5 V) has a peak at a temperature of 750 °C, therefore, this point will be considered as the operating point temperature. The drop in performance beyond 750 °C is probably due to cathode becoming active towards parasitic reactions (methane oxidation) [41]. The OCV has a peak at 600 °C and it drops thereafter, this trend is partly due to less Gibbs free energy available with increasing temperature and partly because of enhanced partial oxidation reaction at anode consuming more oxygen.

4.4. Effect of flow rate

After deducing the results from Fig. 6(a–e), it was found that methane/air ratios of 1:4.76 giving the better performance as compared to other mixing ratios; therefore, the effect of flow rate was analyzed at different temperatures by keeping the mixing ratio as fixed at methane/air of 1:4.76. In Fig. 8, 0.5 V was assumed as the operating cell voltage and the cell current was recorded at different temperatures with increasing mixture flow rates. The maximum current density was found at higher flow rates with a peak at a temperature of 750 °C. It is worth noting to mention here that although

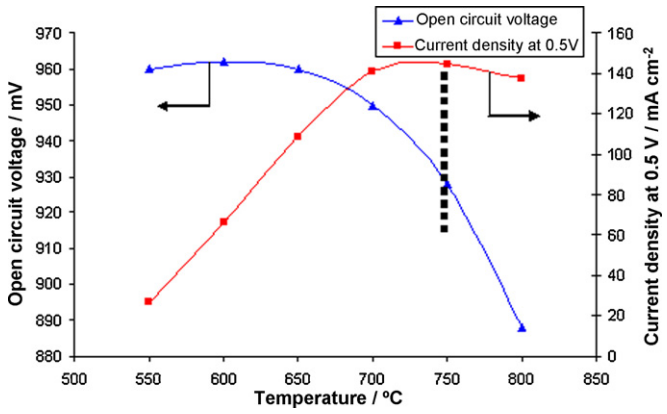

Fig. 7. Temperature vs. OCV and current density at 0.5 V for methane/air mixture of 10/47.6 ml min^{-1}

the current density through the cell increases with increasing flow rate, but this could reduce the cell efficiency due to low utilization at higher flow rates. In order to maintain high electrical efficiencies, either stack of cells can be designed to increase utilization, or, off gas recirculation must be made in stages (cascading) to improve the overall efficiency of the system.

4.5. Effective fuel utilization and effective efficiency

Fuel utilization during fuel cell operation will be a useful tool to estimate the effective performance of the cell. There are two approaches (as shown in Eqs. (1) and (2)) to calculate the fuel utilization reported in the literature [10,11,36,38,69]:

$$\eta_U = \frac{\dot{m}_{f,reacted}}{\dot{m}_{f,in}} = \frac{\frac{M}{z\times F} \times I_{tot}}{\dot{m}_{f,in}} \quad (1)$$

$$\eta_U = 1 - \frac{\dot{m}_{f,out}\Delta h_{f,out}}{\dot{m}_{f,in}\Delta h_{f,in}} \quad (2)$$

where η_U = fuel utilization, $\dot{m}_{f,reacted}$ = mass flow rate of fuel reacted in the cell (kg s^{-1}), $\dot{m}_{f,in}$ = mass of flow rate fuel entering the cell (kg s^{-1}), M = molar mass of reacting fuel (kg mol^{-1}), z = number of electrons participating in the reaction, F = Faraday's constant, 96485 (As mol^{-1}), I_{tot} = total current at the peak power density (A), $\dot{m}_{f,out}$ = mass flow rate of fuel at the outlet (kg s^{-1}), $\Delta h_{f,in}$ = specific enthalpy associated with completely oxidizing the inlet fuel (kJ kg^{-1}), $\Delta h_{f,out}$ = specific enthalpy associated with completely oxidizing the exhaust fuel (kJ kg^{-1}).

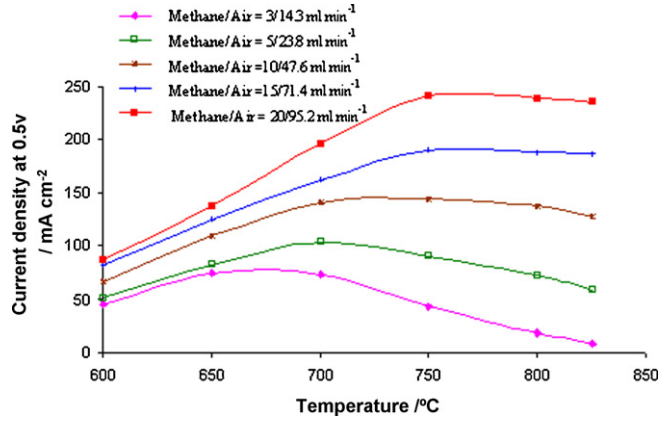

Fig. 8. Temperature vs. current density at 0.5 V for methane/air ratio of 1:4.76 at different flow rates.

Each of these two approaches has merits and limitations, for example: fuel utilization calculated by Eq. (1) only considers the amount of fuel converted into electrical power directly available at the cell or stack (i.e. DC power in front of inverter). This does not take into account, any heating effects i.e. reversible ($T\Delta S$) loss which represents the unavailable energy resulting from the entropy change within the system (for a detailed definition, reader should refer to Ref. [74]), irreversible losses (such as activation, ohmic and concentration polarization), loss of energy (J) equivalent to $2FU_0$ (U_0 = ideal standard voltage; only six electrons participating per electrochemical reaction, in case of single-chamber SOFC utilizing methane/air mixture), part of heat will be carried away by exhaust gases (fuel, inert and product gases), some of the heat can be lost into the environment, some can be stored in cell components. Not only this, the usual tradition of laboratory based experiments requires electrical heating to maintain the cell operating temperature, which further complicates the overall energy balance due to furnace heating. Moreover, not only the various heating losses (as discussed above) are the terms neglected in Eq. (1) but also the current collection efficiency which plays a major role in this calculation is not being taken into account.

The term "Fuel Utilization" as described in Eq. (2) considers the differences in heating values of the inlet and exhaust fuels divided by the heating value of inlet fuel (all based upon completely oxidizing the available fuels). Although, this approach accounts for both the thermal heating and electrical power produced by the cell, calculating the fuel utilization in terms of thermal heat that has not been effectively utilized, makes no sense to consider. For example, in case of a single-cell (where the heat produced is not effectively utilized) it is not worth to consider fuel utilization towards non-effective heat produced. Though, some portion of this heat may be participating in improving the overall system performance via enhancing the local ionic conductivity of the electrolyte, resulting in improved electrical performance, it is very difficult to calculate the effective contribution of this heat. Moreover, calculating the amount of exhaust fuel requires additional equipment such as gas chromatograph (or gas analyser). Furthermore, the outlet fuel is diluted with various product gases, and, one cannot simply use the heating values of various exhausted fuels in concentrated form. Instead, heating values of exhausted fuels must be calculated by considering the dilution factor.

Due to the above complications, we rely our calculations for fuel utilization upon Eq. (1) and term this as "Effective Fuel Utilization" in our experiments – as we did not utilize thermal heat produced and were only interested in electrical output from the cell.

The effective efficiency was calculated by using the following formula [74]:

$$\eta_{eff} = \eta_{ideal} \times \eta_V \times \eta_U \quad (3)$$

where

$$\eta_{ideal} = \frac{U_0}{U_{\Delta H}}, \quad \eta_V = \frac{U_C}{U_0} \quad (4)$$

and η_{eff} = effective efficiency, η_{ideal} = ideal efficiency, η_v = voltage efficiency, U_0 = ideal standard (ΔG°) voltage, $U_{\Delta H}$ = heating voltage and U_C = cell voltage.

The effective fuel utilization and effective efficiencies corresponding to Figs. 6–8 are listed in Tables 2–4, respectively. As can be seen, these values are strongly dependent upon operating temperature, methane/air ratio and fuel flow rate. The highest effective fuel utilization (11.41%) and effective efficiency (5.48%) was obtained at 650 °C, methane/air ratio of 1:4.76 with a fuel flow rate of 3 ml min^{-1}. These extremely low values of fuel utilization and electrical efficiencies (of SC-SOFCs) are one of the major barriers against their practical implementation. During our experiments, it has been observed that this type of design offers more thermal heat

Table 2
Effective fuel utilization and effective efficiency calculated for Fig. 6(a–e) (total flow rate = 12 ml min^{-1}).

CH_4:air	Fuel utilization/effective efficiency (%) at different furnace temperatures				
	550 °C	600 °C	650 °C	700 °C	750 °C
1:4.76	5.13/2.22	7.58/2.55	8.68/3.75	7.94/3.43	7.58/2.55
1:4	4.27/1.64	6.31/2.12	5.19/2.24	6.41/2.16	6.41/1.85
1:3	2.36/1.02	2.85/0.82	2.52/0.72	2.68/0.51	1.95/0.28
1:2	1.46/0.56	2.13/0.61	1.95/0.47	1.65/0.31	1.22/0.17
1:1	0.77/0.26	0.85/0.24	0.97/0.23	0.97/0.18	1.05/0.15

Table 3
Effective fuel utilization and effective efficiency calculated for Fig. 7 (CH_4/air = 10/47.6 ml min^{-1}).

CH_4:air	Fuel utilization/effective efficiency (%) at different furnace temperatures					
	550 °C	600 °C	650 °C	700 °C	750 °C	800 °C
1:4.76	1.24/0.59	3.05/1.46	5.01/2.40	6.5/3.12	6.65/3.19	6.33/3.04

Table 4
Effective fuel utilization and effective efficiency calculated for Fig. 8 (CH_4:air = 1:4.76).

CH_4/air (ml min^{-1})	Fuel utilization/effective efficiency (%) at different furnace temperatures					
	600 °C	650 °C	700 °C	750 °C	800 °C	825 °C
3/14.3	6.92/3.33	11.41/5.48	11.24/5.40	6.52/3.13	2.85/1.37	1.22/0.58
5/23.8	4.64/2.23	7.58/3.64	9.53/4.58	8.31/3.99	6.60/3.17	5.37/2.58
10/47.6	3.05/1.46	5.01/2.40	6.50/3.12	6.65/3.19	6.33/3.04	5.86/2.82
15/71.4	2.54/1.22	3.83/1.84	4.97/2.39	5.83/2.80	5.77/2.77	5.75/2.76
20/95.2	2.00/0.96	3.17/1.52	4.52/2.17	5.55/2.66	5.50/2.64	5.42/2.60

as compared to electrical power, suggesting their potential use in combined heat and power (CHP) applications. Shao et al. [9] in their experiments effectively used this thermal heat to sustain the fuel cell temperature in the absence of external heat source.

Liu et al. [10] have suggested some ways to improve the fuel utilization, we add some more. For example, increasing the gas velocity with a nozzle for injecting air/fuel mixture in to the gas-chamber or by reducing the diameter of the gas-chamber tube, exhaust gas re-circulation in cascading, combustion of exhaust air/fuel mixture in an after-burner and utilize the produced heat either for CHP purpose or to pre-heat the inlet air/fuel mixture to the gas-chamber.

4.6. Output performance

The cell performance was compared (as shown in Fig. 9) with dual-chamber hydrogen operated (750 °C, 20 ml min^{-1}), dual-chamber methane operated (750 °C, 5 ml min^{-1}) and single-chamber methane/air operated (750 °C, 20/95.2 ml min^{-1}) micro-tubular cell. In dual-chamber configuration the fuel was supplied to the anode and the cathode was exposed to ambient air, whereas for single-chamber condition, both the anode and the cathode were supplied with same air-fuel mixture. Since it is not wise to compare different fuels with same flow rates (because each fuel has its own heating value, different number of electrons participating in the reaction and different mechanism to produce electrical power), therefore for hydrogen and methane, the flow rates were chosen from [72,73] for an optimum performance of a micro-tubular cell of same dimensions used in this study. The maximum power density (p_{max}) of hydrogen (dual-chamber), methane (dual-chamber) and methane/air (single-chamber) at an operating voltage of 0.5 V was 385, 293 and 122 mW cm^{-2}, respectively. It shows that the cell performance under methane/air operated single-chamber conditions is approximately three times lower than that of hydrogen operated dual-chamber cell. This shows that even without optimization of microstructure, flow management, fuel utilization and selectiveness of the electrodes, the single-chamber conditions can provide an acceptable level of performance. Further studies are required to optimize these parameters in order to boost the performance closer to that of dual-chamber configuration.

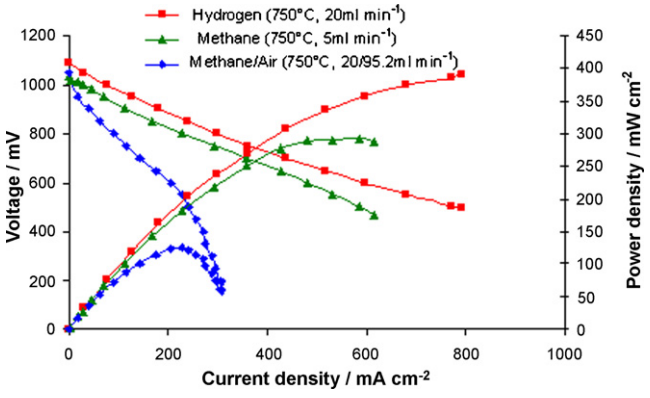

Fig. 9. Performance curve for hydrogen (dual-chamber), methane (dual-chamber) and methane/air (single-chamber) as a fuel.

In Table 5, a summary of earlier work on SC-SOFCs done by many researchers has been reported. Although, it will not be appropriate to compare this study with the work done by other groups due to different manufacturing techniques (electrode/electrolyte microstructure, thickness, sintering temperature), operating temperature, flow rates, mixing ratio etc., still it will worth to have a quick look on those using the same conventional materials. Studies based upon using the same conventional materials (i.e. Ni-YSZ/YSZ/LSM), same SC-SOFC type (Hibino B-type [41]) and same fuel (methane) highlight the following [13,23,24,36,37,63]:

- In this present study, the lowest fuel flow rate (20 ml min^{-1} with methane/air ratio of 1:4.76) is used.
- The total flow rate is also the lowest in this study (115.2 ml min^{-1} with methane/air ratio of 1:4.76).
- The OCV obtained in this study is the highest (1.05 V) at 750 °C with methane/air ratio of 1:4.76. The same OCV was also obtained

Table 5
Performances of SC-SOFCs reported by various research groups.

Fuel	Type[a]	Anode	Electrolyte	Cathode	Electrolyte thickness (mm)	Furnace temperature (°C)	OCV (mV)	p_{max} (mW cm^{-2})	R_{mix}	Total flow rate (mW cm^{-2})	η_U (%)	Ref.
C_3H_8	B	Ni-SDC	SDC	BSCF-SDC	0.02	500	ca. 700	440	0.44	490	–	[6]
CH_4	C	Pd	BaCeGd	Au	1.0	950	700	-	2.0	300	–	[7]
C_4H_{10}	B	Ni-SDC	SDC	SSC	0.15	300	800	38	0.5	300	–	[8]
C_3H_8	B	Ni-SDC	SDC	BSCF-SDC	0.02	500	700	247	0.44	490	–	[9]
CH_4	B	Ni-YSZ	YSZ	LSM(SDC)[g]	0.015	700	1820[k]	371[k]	1.0	400	~1.0	[10]
CH_4	B	Ni-YSZ	YSZ	LSCF	0.001-0.002	750	830	120	ca. 1.0	300	2.4	[11]
C_3H_8	B	Ni-SDC	SDC	SSC-SDC	0.01	525	650	210	0.4	540	–	[12]
C_3H_8	B	Ni-SDC	SDC	SSC-SDC	0.01	525	750	185	0.33	160	–	[12]
CH_4	B	Ni-YSZ	YSZ	LSM	0.008	600	940	220	1.0	450	–	[13]
C_2H_6	B	Ni-SDC	SDC	SSC	0.15	500	920	403	1.0	300	–	[14]
CH_4	B	Ni-SDC	GDC-BCY-GDC	SSC	0.003	500	ca. 880	302	2.0	300	–	[15]
CH_4	C	Ni-YSZ	YSZ	LSM	–	770	500	1	-	-	–	[16]
CH_4	C	Ni-YSZ	YSZ	LSM	0.2	800	850	40	2.0	350	–	[17]
CH_4	C	Ni-YSZ	YSZ	LSM	1.0	800	615	1.2	ca. 1.48	245	–	[18]
CH_4	C	Ni-GDC	YSZ	LSM[h]	0.5	950	ca. 800	102	1.0	300	–	[22]
CH_4	B	Ni-GDC	YSZ	LSM[h]	0.3	950	ca. 810	204	1.0	300	–	[22]
CH_4	B	Ni-YSZ	YSZ	LSM	0.008	750	915	100	ca. 2.0	400	–	[23]
CH_4	B	Ni-YSZ	YSZ	LSM(SDC)[g]	0.008	750	968	404	ca. 2.0	400	–	[23]
CH_4	B	Ni-YSZ	YSZ	LSM	0.2	800	1020	85	-	-	–	[24]
CH_4	C	Ni-GDC	GDC	SSC	–	650	770	17	2.0	100	–	[25]
CH_4	B	Ni-SDC-Pd	SDC	SSC	0.15	550	ca. 800	644	2.0	300	–	[26]
CH_4	B	Ni-SDC	SDC	BSCF-SDC	0.02	650	710	760	ca. 1.08	487	–	[27]
C_3H_8	B	Ni-YSZ	YSZ	LSCF	0.1	600	800	-	ca. 0.53	300	–	[28]
C_3H_8	B	Ni-GDC	YSZ	LSCF	0.1	600	800	-	ca. 0.53	300	–	[28]
C_3H_8	B	Ni-SDC	YSZ	LSCF	0.1	600	800	-	ca. 0.53	300	–	[28]
CH_4	B	Ni-GDC	YSZ[c]	LSM[h]	0.3	950	845	256	1.0	300	–	[29]
CH_4	C	Ni-GDC	YSZ[c]	LSM[h]	0.3	950	800	143	1.0	300	–	[29]
CH_4	C	Ni-GDC-Pd	YSZ	LSM-GDC	–	900	804	101.2	ca. 3.57	240	–	[30]
CH_4	B	Pt	BCY	Au	0.5	950	ca. 800	170	2.0	210	–	[31]
C_4H_{10}	C	Ni-SDC-Pd	SDC	SSC	2.0	600	ca. 800	ca. 245	ca. 0.53	300	–	[32]
C_2H_6	C	Ni-SDC	SDC	SSC	2.0	600	ca. 800	ca. 75	ca. 1.13	300	–	[32]
CH_4	B	Pt -(MnO_2)	YSZ[d]	Au[i]	0.5	950	ca. 600	50.4	1.0	300	–	[33]
CH_4	C	Pd	BaCeGd	Au	-	950	700	-	2.0	300	–	[35]
CH_4	B	Ni-YSZ	YSZ	LSM	0.2	800	860	360	0.88	350	–	[36]
CH_4	B	Ni-YSZ	YSZ	LSM	0.01	800	1050	260	2.0	350	–	[37]
CH_4	B	Ni-YSZ	YSZ[e]	LSCF	0.018	606	780	660	1.0	900	~5.0	[38]
CH_4	B	Pt	YSZ[f]	Au	-	950	-	3	2.0	120	–	[39]
CH_4	B	Pt	YSZ[f]	Au	0.5	950	700	34	2.0	210	–	[40]
C_3H_8	B	Ni-SDC	SDC	LSCF-SDC	0.5	650	780	210	ca. 0.53	300	–	[42]
C_3H_8	B	Ni-SDC	SDC	LSCF-SDC	0.5	575	800	111.12	ca. 0.53	300	–	[44]
C_3H_8	B	Ni-SDC	SDC	SSC-SDC	0.8	600	720	18.5	ca. 0.53	300	0.37	[45]
C_4H_{10}	B	Ni-SDC	GDC	SSC	0.015	300	921	176	0.5	300	–	[46]
C_4H_{10}	B	Ni-SDC-Ru	GDC	SSC	0.015	200	ca. 900	44	0.5	300	–	[46]
CH_4	B	Ni	YSZ	LSM	1.0	950	ca. 795	121	1.0	300	–	[47]
CH_4	B	Ni-LSCM	BLI	SSC	0.5	800	657	64.7	ca. 4.76	200	–	[48]
CH_4	C	Ni-SDC	YSZ	LSM	1.0	900	355	73.5	ca. 3.57	280	–	[49]
C_2H_6	B	Ni-SDC	LSGM	SSC	0.18	600	ca. 1000	ca. 350	1.0	300	–	[50]
CH_4	B	Ni-GDC	GDC	SSC	0.29	600	ca. 680	468	1.6	1500	–	[51]
C_4H_{10}	B	Ni-SDC	GDC	SSC	0.015	300	ca. 900	59	0.5	350	–	[52]
DME[b]	B	Ni-SDC-Ru	GDC	SSC	0.015	300	ca. 771	64	1.8	350	<2.0	[52]
Ethanol	B	Ni-SDC-Cu/Zn/Al	GDC	SSC	0.015	300	811	117	0.4	350	<2.0	[52]
CH_4	B	Ni-SDC	GDC	BSCF-SDC	0.015	650	710	760	ca. 1.16	462	–	[58]
CH_4	C	Ni-YSZ	YSZ	LSM[j]	0.2	700	ca. 900	2.3	2.0	150	–	[63]
CH_4	B	Ni-YSZ	YSZ	LSM	0.5	700	925	ca. 200	1.0	450	–	[63]

Table 5 (*Continued*)

Fuel	Type[a]	Anode	Electrolyte	Cathode	Electrolyte thickness (mm)	Furnace temperature (°C)	OCV (mV)	p_{max} (mW cm^{-2})	R_{mix}	Total flow rate (mW cm^{-2})	η_U (%)	Ref.
CH_4	C	Ni-YSZ	YSZ	LSM[j]	0.2	700	ca. 800	1.3	2.0	150	–	[64]
CH_4	B	Ni-SDC	SDC	BSCF-SDC	0.02–0.03	600	ca. 740	570	ca. 1.13	470	–	[65]
CH_4	B	Ni-SDC	SDC	BSCF-SDC	0.02–0.03	600	ca. 740	570	ca. 1.13	470	–	[65]
CH_4	C	Ni-YSZ	YSZ	LSM[j]	0.2	700	961	9.37	2.0	150	–	[66]
CH_4	B	Ni-YSZ	YSZ	LSM[j]	0.015	750	1050	122	1.0	115.2	5.55	This study

[a] Type = A, B and C as defined in Ref. [41].
[b] DME = dimethyl ether.
[c] YSZ dipped into $(MnNO_3)_2$.
[d] YSZ modified with 1 wt% MnO_2.
[e] Porous YSZ.
[f] Pr doped YSZ.
[g] SDC impregnated LSM.
[h] LSM modified with 15 wt% MnO_2.
[i] Au modified with 20 wt%MnO_2.
[j] Active layer of LSM-YSZ prior to LSM cathode.
[k] Two cell stack.

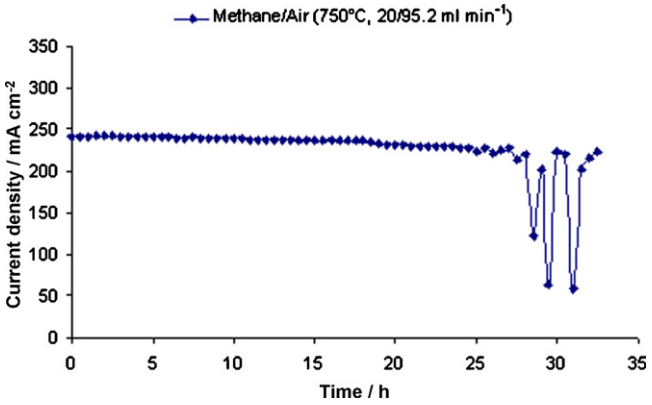

Fig. 10. Stability test for current density at 0.5 V vs. time in hours.

by Napporn and co-workers [37] at 800 °C using methane/air mixture (methane/oxygen ratio of 2.0), however the total flow rate used in their study was relatively high i.e. 350 ml min^{-1}.

- The highest power density reported was 360 mW cm^{-2} at 800 °C using methane/air mixture (methane/oxygen ratio of 0.88) with a total flow rate of 350 ml min^{-1} [36]. Since the flow rate used for obtaining this power density was rather high, we made an attempt to compare our results with a relatively comparable flow rates used in our study. In Fig. 9 of Ref. [36], authors used a total flow rate of 150 ml min^{-1} (methane/oxygen ratio of 0.63) at 800 °C. This corresponds to approximately 17.5 ml min^{-1} of methane and 132.5 ml min^{-1} air, giving ca.140 mW cm^{-2}. However, the methane/oxygen ratio of 0.63 comes in the explosive range of 5–15% methane by volume in air, which is not practical for working at higher flow rates. In comparison to this, our study employs 20 ml min^{-1} of methane and 95.2 ml min^{-1} air, giving approximately 122 mW cm^{-2} at a slightly lower temperature (750 °C) to that of used in Ref. [36]. The total flow rate used in our study was also slightly lower (115.2 ml min^{-1}) and the methane/air mixture (methane to oxygen ratio of 1.0) employed was relatively safe. Therefore, this study confirms that the micro-tubular design can offer some advantages in terms of higher OCV and comparable performance.

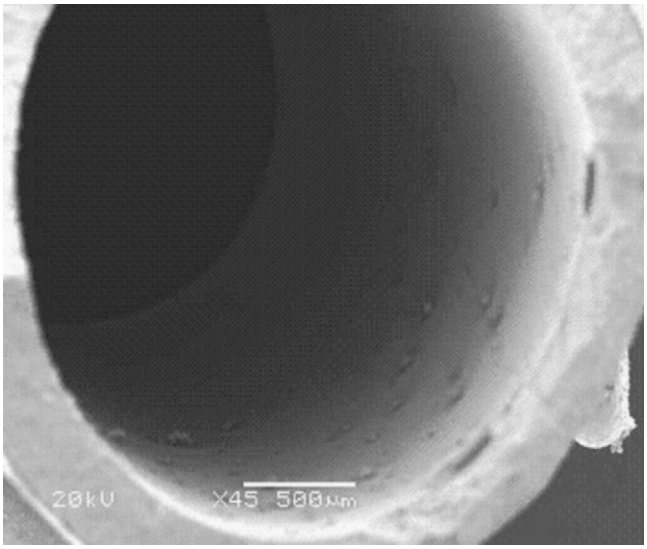

Fig. 11. SEM photograph of anode surface after operation of 32 h at methane/air ratio of 1:4.76.

4.7. Stability

The cell stability was monitored at a methane/air ratio of 1:4.76 (at 0.5 V) for 32 h. Initially, up to 24 h the degradation in the cell performance was 0.05%, thereafter, oscillations (of increasing magnitude with respect to time) in current density were observed (Fig. 10). This shows that although, 1:4.76 was giving the best *I–V* curves (as shown above) but its performance was not stable and therefore this mixing ratio must be avoided, probably re-oxidizing the anode with high amount of air present in the mixture. The cell was taken out of the chamber and the anode surface was analyzed by scanning electron microscopy (SEM). Fig. 11 shows pitting of the anode surface possibly due to oxidation–reduction cycles on anode surface resulting in loss of nickel as reported by Kuhn et al. [66].

5. Conclusions

We summarize the conclusions into the following sentences:

- Anode was successfully reduced by using methane/air mixture ratio (1:2.4) at a temperature of 750 °C but it took approximately 9 h to reduce the anode and also the current drawn through the cell was lower.
- Although methane/air mixture ratio of 1:4.76 gives best performance at all operating temperature ranges studied, however, the degradation test shows that operating at such a mixing ratio cannot run longer than 24 h. Thereafter, oxidation–reduction of nickel is expected and fluctuations in current density are observed.
- Output performance increases with increase in flow rate but this could reduce the fuel utilization and thus current efficiency of the cell. In order to improve utilization and efficiency, the cells must be operated in stack.
- Comparison of hydrogen, methane and methane/air mixture operated cell shows that the cell can give one-third power output in single-chamber conditions without any optimization and selectiveness of the cell materials.
- Anode surface was damaged after oxidation–reduction cycles due to operation at a methane/air ratio of 1:4.76, and pitting of the anode material is clearly observed.

Further research is on going to investigate into the degradation mechanism at various mixing ratios and the results will follow in future publications.

Acknowledgments

The authors would like to thank E.ON-UK for funding Mr. Naveed Akhtar through Dorothy Hodgkin Postgraduate Award (DHPA) scheme. We are also very grateful to Professor Ludger Blum, Head of Department, Fuel Cell Process Engineering, Research Centre Juelich, Germany for valuable discussion on fuel utilization.

References

[1] S.C. Singhal, K. Kendall, High Temperature Solid Oxide Fuel Cells: Fundamentals Design and Applications, Elsevier, Kidlington Oxford, 2003, pp. 1.
[2] W. Bujalski, J. Paragreen, G. Reade, S. Pyke, K. Kendall, J. Power Sources 157 (2006) 745–749.
[3] W. Bujalski, C.M. Dikwal, K. Kendall, J. Power Sources 171 (2007) 96–100.
[4] V.A. Restrepo, J.M. Hill, Appl. Catal. A 342 (2008) 49–55.
[5] S. Ghosh, A.D. Sharma, P. Kundu, S. Mahanty, R.N. Basu, J. Non-Cryst. Solids 354 (2008) 4081–4088.
[6] Z. Shao, S.M. Haile, Nature 431 (2004) 170–173.
[7] T. Hibino, K. Ushiki, T. Sato, Y. Kuwahara, Solid State Ionics 81 (1995) 1–3.
[8] T. Hibino, A. Hashimoto, T. Inoue, J. Tokuno, S. Yoshida, M. Sano, J. Electrochem. Soc. 148 (2001) A544–A549.
[9] Z. Shao, S.M. Haile, J. Ahn, P.D. Ronney, Z. Zhan, S.A. Barnett, Nature 435 (2005) 795–798.
[10] M. Liu, Z. Lü, B. Wei, R. Zhu, X. Huang, K. Chen, G. Ai, W. Su, J. Electrochem. Soc. 154 (2007) B588–B592.
[11] T. Suzuki, P. Jasinski, V. Petrovsky, H.U. Anderson, F. Dogan, J. Electrochem. Soc. 151 (2004) A1473–A1476.
[12] Z. Shao, C. Kwak, S.M. Haile, Solid State Ionics 175 (2004) 39–46.
[13] B. Morel, R. Roberge, S. Savoie, T.W. Napporn, M. Meunier, Appl. Catal. A 323 (2007) 181–187.
[14] T. Hibino, A. Hashimoto, T. Inoue, J. Tokuno, S. Yoshida, M. Sano, Science 288 (2000) 2031–2033.
[15] A. Tomita, S. Teranishi, M. Nagao, T. Hibino, M. Sano, J. Electrochem. Soc. 153 (2006) A956–A960.
[16] J.-P. Viricelle, C. Pijolat, B. Riviere, D. Rotureau, D. Briand, N.F. de Rooij, Sens. Actuators B 118 (2006) 263–268.
[17] X.J. -Bedard, T.W. Napporn, R. Roberge, M. Meunier, J. Electrochem. Soc. 154 (2007) B305–B309.
[18] D. Rotureau, J.-P. Viricelle, N. Caillol, M. Pijolat, D. Rotureau, D. Briand, J. Electrochem. Soc. 25 (2005) 2633–2636.
[19] B. Morel, R. Roberge, S. Savoie, T.W. Napporn, M. Meunier, Electrochem. Solid-State Lett. 10 (2007) B31–B33.
[20] S.-J. Ahn, Y.-B. Kim, J. Moon, J.-H. Lee, J. Kim, J. Electroceram. 17 (2006) 689–693.
[21] J. Fleig, H.L. Tuller, J. Maier, Solid State Ionics 174 (2004) 261–270.
[22] T. Hibino, S. Wang, S. Kakimoto, M. Sano, Solid State Ionics 127 (2000) 89–98.
[23] B. Wei, Z. Lü, X. Huang, M. Liu, K. Chen, W. Su, J. Power Sources 167 (2007) 58–63.
[24] T.W. Napporn, F. Morin, M. Meunier, Electrochem. Solid-State Lett. 7 (2004) A60–A62.
[25] B.E. Buergler, M. Ochsner, S. Vuillemin, L.J. Gauckler, J. Power Sources 171 (2007) 310–320.
[26] T. Hibino, A. Hashimoto, M. Yano, M. Suzuki, S. Yoshida, M. Sano, J. Electrochem. Soc. 149 (2002) A133–A136.
[27] Z. Shao, J. Mederos, W.C. Chueh, S.M. Haile, J. Power Sources 162 (2006) 589–596.
[28] P. Jasinski, T. Suzuki, F. Dogan, H.U. Anderson, Solid State Ionics 175 (2004) 35–38.
[29] T. Hibino, H. Tsunekawa, S. Tanimoto, M. Sano, J. Electrochem. Soc. 147 (2000) 1338–1343.
[30] S.-J. Ahn, Y.-B. Kim, J. Moon, J.-H. Lee, J. Kim, J. Power Sources 171 (2007) 511–516.
[31] K. Asano, T. Hibino, H. Iwahara, J. Electrochem. Soc. 142 (1995) 3241–3245.
[32] T. Hibino, A. Hashimoto, M. Suzuki, M. Yano, S. Yoshida, M. Sano, J. Electrochem. Soc. 149 (2002) A195–A200.
[33] T. Hibino, Y. Kuwahara, S. Wang, J. Electrochem. Soc. 146 (1999) 2821–2826.
[34] B. Zhu, G. Meng, B.-E. Mellander, J. Power Sources 79 (1999) 30–36.
[35] T. Hibino, K. Ushiki, Y. Kuwahara, Solid State Ionics 91 (1996) 69–74.
[36] T.W. Napporn, X.J. Bedard, F. Morin, M. Meunier, J. Electrochem. Soc. 151 (2004) A2088–A2094.
[37] X.J. Bedard, T.W. Napporn, R. Roberge, M. Meunier, J. Power Sources 153 (2006) 108–113.
[38] T. Suzuki, P. Jasinski, V. Petrovsky, H.U. Anderson, F. Dogan, J. Electrochem. Soc. 152 (2005) A527–A531.
[39] L. Bay, T. Horita, N. Sakai, M. Ishikawa, K. Yamaji, H. Yokokawa, Solid State Ionics 113–115 (1998) 363–367.
[40] K. Asano, H. Iwahara, J. Electrochem. Soc. 144 (1997) 3125–3130.
[41] M. Yano, A. Tomita, M. Sano, T. Hibino, Solid State Ionics 177 (2007) 3351–3359.
[42] T. Suzuki, P. Jasinski, H.U. Anderson, F. Dogan, J. Electrochem. Soc. 151 (2004) A1678–A1682.
[43] I. Riess, Solid State Ionics 177 (2006) 1591–1596.
[44] T. Suzuki, P. Jasinski, H.U. Anderson, F. Dogan, Electrochem. Solid-State Lett. 7 (2004) A391–A393.
[45] I.C. Stefan, C.P. Jacobson, S.J. Visco, L.C. De Jonghe, Electrochem, Solid- State Lett. 7 (2004) A198–A200.
[46] A. Tomita, D. Hirabayashi, T. Hibino, M. Nagao, M. Sano, Electrochem. Solid-State Lett. 8 (2005) A63–A65.
[47] T. Hibino, S. Wang, S. Kakimoto, M. Sano, Electrochem. Solid-State Lett. 2 (1999) 317–319.
[48] S. Asahara, D. Michiba, M. Hibino, T. Yao, Electrochem. Solid-State Lett. 8 (2005) A449–A451.
[49] S.-J. Ahn, J.-H. Lee, J. Kim, J. Moon, Electrochem. Solid-State Lett. 9 (2006) A228–A231.
[50] T. Hibino, A. Hashimoto, T. Inoue, J. Tokuno, S. Yoshida, M. Sano, J. Electrochem. Soc. 147 (2000) 2888–2892.
[51] B.E. Buergler, M.E. Siegrist, L.J. Gauckler, Solid State Ionics 176 (2005) 1717–1722.
[52] M. Yano, T. Kawai, K. Okamoto, M. Nagao, M. Sano, A. Tomita, T. Hibino, J. Electrochem. Soc. 154 (2007) B865–B870.
[53] I. Riess, P.J. van der Put, J. Schoonman, Solid State Ionics 82 (1995) 1–4.
[54] S. Raz, M.J.G. Jak, J. Schoonman, I. Riess, Solid State Ionics 149 (2002) 335–341.
[55] I. Riess, Solid State Ionics 176 (2005) 1667–1674.
[56] B.E. Buergler, A.N. Grundy, L.J. Gauckler, J. Electrochem. Soc. 153 (2006) A1378–A1385.
[57] Y. Hao, D.G. Goodwin, J. Electrochem. Soc. 154 (2007) B207–B217.
[58] Y. Hao, Z. Shao, J. Mederos, W. Lai, D.G. Goodwin, S.M. Haile, Solid State Ionics 177 (2006) 2013–2021.
[59] C.-Y. Chung, Y.-C. Chung, J. Power Sources 154 (2006) 35–41.
[60] C.-Y. Chung, Y.-C. Chung, J. Kim, J. Lee, H.W. Lee, J. Electroceram. 17 (2006) 959–964.
[61] N. Akhtar, S.P. Decent, D. Loghin, K. Kendall, ASME 6th International Fuel Cell Science, Engineering and Technology Conference, June 16–18, Denver, Colorado, U.S.A., 2008.

[62] N. Akhtar, S.P. Decent, D. Loghin, K. Kendall, 8th European SOFC Forum 30 June–4 July, 2008 Lucerne, Switzerland.
[63] M. Kuhn, T. Napporn, M. Meunier, D. Therriault, S. Vengallatore, J. Power Sources 177 (2008) 148–153.
[64] M. Kuhn, T. Napporn, M. Meunier, S. Vengallatore, D. Therriault, J. Micromech. Microeng. 18 (2008) 015005.
[65] C. Zhang, Y. Zheng, R. Ran, Z. Shao, W. Jin, N. Xu, J. Ahn, J. Power Sources 179 (2008) 640–648.
[66] M. Kuhn, T.W. Napporn, M. Meunier, D. Therriault, J. Electrochem. Soc. 155 (2008) B994–B1000.
[67] I. Riess, J. Power Sources 175 (2008) 325–337.
[68] M. Yano, M. Nagao, K. Okamoto, A. Tomita, Y. Uchiyama, N. Uchiyama, T. Hibino, Electrochem. Solid-State Lett. 11 (2008) B29–B33.
[69] Y. Hao, D.G. Goodwin, J. Power Sources 183 (2008) 157–163.
[70] Y. Hao, D.G. Goodwin, J. Electrochem. Soc. 155 (2008) B666–B674.
[71] C. Mallon, K. Kendall, J. Power Sources 145 (2005) 154–160.
[72] A. Dhir, K. Kendall, J. Power Sources 181 (2008) 297–303.
[73] T.J. Lee, K. Kendall, J. Power Sources 181 (2008) 195–198.
[74] EG&G Technical Services Inc., Fuel Cell Handbook, 7th ed., U.S. Department of Energy, Office of Fossil Energy, National Energy Technology Laboratory, 2004, pp. 2–9.